

# CMFDFormer: Transformer-based Copy-Move Forgery Detection with Continual Learning

Yaqi Liu, Chao Xia, Song Xiao, Qingxiao Guan, Wenqian Dong, Yifan Zhang, Nenghai Yu

**Abstract**—Copy-move forgery detection aims at detecting duplicated regions in a suspected forged image, and deep learning based copy-move forgery detection methods are in the ascendant. These deep learning based methods heavily rely on synthetic training data, and the performance will degrade when facing new tasks. In this paper, we propose a Transformer-style copy-move forgery detection network named as CMFDFormer, and provide a novel PCSD (Pooled Cube and Strip Distillation) continual learning framework to help CMFDFormer handle new tasks. CMFDFormer consists of a MiT (Mix Transformer) backbone network and a PHD (Pluggable Hybrid Decoder) mask prediction network. The MiT backbone network is a Transformer-style network which is adopted on the basis of comprehensive analyses with CNN-style and MLP-style backbones. The PHD network is constructed based on self-correlation computation, hierarchical feature integration, a multi-scale cycle fully-connected block and a mask reconstruction block. The PHD network is applicable to feature extractors of different styles for hierarchical multi-scale information extraction, achieving comparable performance. Last but not least, we propose a PCSD continual learning framework to improve the forgery detectability and avoid catastrophic forgetting when handling new tasks. Our continual learning framework restricts intermediate features from the PHD network, and takes advantage of both cube pooling and strip pooling. Extensive experiments on publicly available datasets demonstrate the good performance of CMFDFormer and the effectiveness of the PCSD continual learning framework.

**Index Terms**—Copy-move forgery detection, Transformer, pluggable hybrid decoder, continual learning, pooled cube and strip distillation.

## I. INTRODUCTION

**D**IGITAL image forensics has been drawing more and more attention in the scientific and industrial communities for the urgent needs to detect forged digital images [1]. Forged digital images are not only used for innocent purposes, but also used for disrupting public opinion, political order or other criminal aims by ill-disposed forgers [2]. Copy-move forgery is one common manipulation among various digital image forgeries, and it duplicates regions in the same images in order to hide or reinforce objects of interest. Copy-move

This work was supported in part by NSFC under Grant 62102010, and in part by the Fundamental Research Funds for the Central Universities under Grant 3282023016.

Y. Liu, C. Xia, S. Xiao, Y. Zhang are with Beijing Electronic Science and Technology Institute, Beijing 100070, China (e-mail: liuyaqi@besti.edu.cn; xiachao@besti.edu.cn; xiaosong@mail.xidian.edu.cn).

Q. Guan is with the Computer Engineering College, Jimei University, Xiamen 361021, China (e-mail: 258817567@qq.com).

W. Dong is with the State Key Laboratory of Integrated Service Network, Xidian University, Xi'an 710071, China (e-mail: wqdong@xidian.edu.cn).

N. Yu is with the CAS Key Laboratory of Electro-magnetic Space Information, University of Science and Technology of China, Hefei 230026, China (e-mail: ynh@ustc.edu.cn).

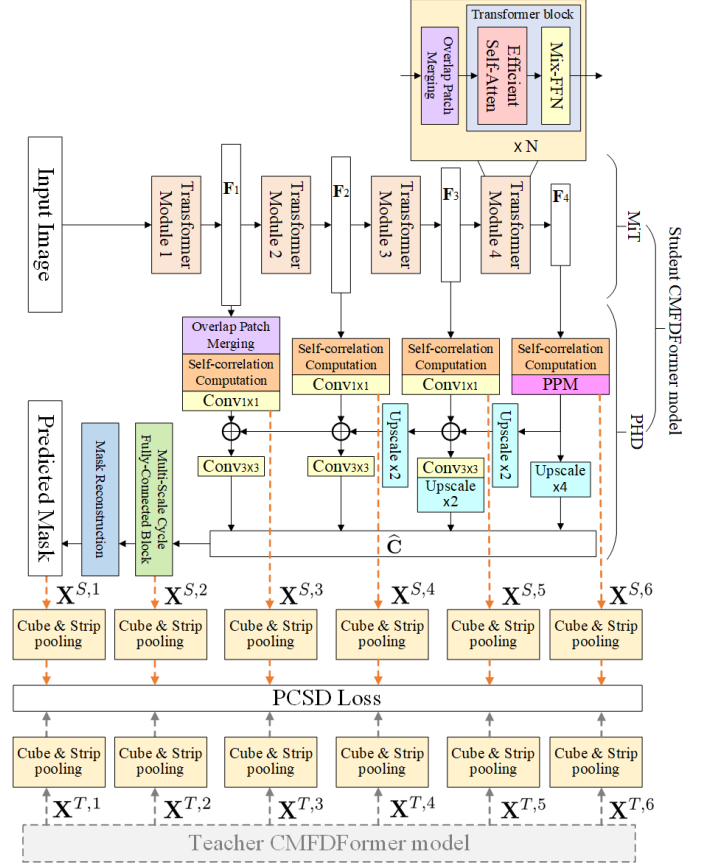


Fig. 1. Overview of CMFDFormer and PCSD continual learning.

forgery detection, which aims to identify duplicated regions, has always been a hot topic in digital image forensics [3].

Conventional copy-move forgery detection methods, which are designed based on hand-crafted features, have dominated this field in the past [3]. While in recent years, deep learning based methods have been in the ascendant [4]–[7]. As the pioneering approach [4], ButsterNet builds an end-to-end trainable deep neural network which features a two-branch architecture followed by a fusion module. It not only detects duplicated regions but also distinguishes source/target regions. In [5], Dense-InceptionNet was constructed for copy-move forgery detection by combining pyramid feature extractor blocks to extract the multi-dimensional and multi-scale dense-features. In [6], Chen et al. proposed two serially constructed subnetworks: one for copy-move similarity detection, and the other for source/target region distinguishment based on similarity detection results. In [7], Liu et al. concentrated

on the similarity detection problem, and proposed a two-stage framework which combines self deep matching and keypoint matching through a proposal selection module. All these methods are constructed based on Convolutional Neural Networks (CNN). Transformer-style [8]–[10] and MLP-style (Multi-Layer Perceptron) [11]–[13] networks recently attract an ever increasing attention for many computer vision tasks. In the field of copy-move forgery detection, the feasibility of constructing Transformer-style and MLP-style backbones is still an open issue. We construct three styles (i.e., CNN, Transformer, MLP styles) of networks with a novel pluggable hybrid decoder, making a comparative analysis. Besides, deep learning based copy-move forgery detection methods face a major problem: they tend to rely on the synthetic training datasets and have a poor generalization ability in realistic testing datasets which may have different distributions with training datasets. We propose to use continual learning mechanisms [14]–[17] to alleviate this problem.

In this paper, we propose a Transformer-style copy-move forgery detection network, i.e., CMFDFormer, and a novel PCSD (Pooled Cube and Strip Distillation) continual learning framework for copy-move forgery detection. The main architecture is shown in Fig. 1. CMFDFormer mainly consists of a MiT (Mix Transformer) feature extractor and a PHD (Pluggable Hybrid Decoder) mask prediction network. Our motivation of adopting Transformer is that copy-move forgery detection needs to compare all pairs of blocks or regions in one image, the accumulated affinity matrix computation using key-query multiplication in Transformer is helpful for capturing visual similarity features. And the MiT backbone is selected based on comprehensive analyses among ResNet (CNN-style) [18], CycleMLP (MLP-style) [19], and MiT (Transformer-style) [20]. Then, we propose a PHD network to generate the predicted mask making use of backbone features. In PHD, we utilize self-correlation computation to detect similar features, and construct a hierarchical feature integration block to get a feature map  $\hat{C}$  with rich hierarchical information. And, we propose a multi-scale cycle fully-connected block making use of Cycle FCs with different dilation rates to investigate multi-scale information from  $\hat{C}$ . Finally, we construct a mask reconstruction block to get the predicted mask. This network is named as Pluggable Hybrid Decoder (PHD) for that it takes advantage of step-by-step hybrid blocks and is adaptable for different style backbones to achieve comparable performance.

Besides, we propose a PCSD continual learning framework for copy-move forgery detection. Deep learning based copy-move forgery detection methods are confronted with a severe domain shift problem. Specifically, the deep learning based methods heavily rely on the training datasets, and can not achieve satisfied results on different testing datasets. While simply finetuning on different testing datasets can cause catastrophic forgetting [14]. In another word, the finetuned model can not simultaneously achieve good performance on former data and finetuning data. (Finetuning is commonly seen in the task of image forgery localization which also faces the catastrophic forgetting problem [2].) We propose a PCSD continual learning framework to make sure our model can achieve comparable performance on both old tasks and new

tasks. Our PCSD continual learning framework is different from other continual learning methods in which they adopt intermediate features from feature extractors for knowledge distillation [15]. We find that if we use backbone intermediate features, it is difficult to converge for continual learning in copy-move forgery detection. Thus, our framework adopts features in PHD after self-correlation computation. Besides, we design a PCSD loss in which cube pooling and strip pooling are simultaneously conducted to capture features from both multi-scale square regions and long-range banded regions. In summary the main contributions of our work are three-fold:

- A novel Transformer-style copy-move forgery detection network, i.e., CMFDFormer, is proposed, on the basis of comprehensively analysing CNN-style, MLP-style and Transformer-style backbones.
- A PHD network is proposed for mask prediction. By incorporating self-correlation computation, hierarchical feature integration, multi-scale Cycle FC and mask reconstruction blocks, our PHD is applicable to backbones of different styles, achieving comparable performance.
- A PCSD continual learning framework is proposed for copy-move forgery detection. To the best of our knowledge, our study is the first to cope with the domain shift problem in copy-move forgery detection by formulating a continual learning framework.

## II. RELATED WORK

In this section, we briefly review the state-of-the-art copy-move forgery detection methods, Transformer-style networks, MLP-style networks and continual learning mechanisms which are the key techniques researched in our work.

### A. Copy-Move Forgery Detection

In recent decades, copy-move forgery detection has been a hot topic in digital image forensics. Different from other image forgery detection and localization tasks which need to detect high-level [21] or low-level [22]–[24] inconsistencies, copy-move forgery detection detects visual similar regions in candidate images. Conventional copy-move forgery detection methods can be categorized into two groups: 1) dense-field (or block-based) methods [25]–[28] and 2) sparse-field (or keypoint-based) methods [3], [29]–[33]. Dense-field methods divide investigated images into regular and overlapped blocks, and adopt numerous hand-crafted block features. Although dense-field methods are more accurate, the robustness against distortions still needs to be improved, and dense-field methods also have higher complexity. In sparse-field methods, SIFT (Scale Invariant Feature Transform) [3], [29], [30] and SURF (Speeded-Up Robust Features) [31], [32] are commonly adopted for sparse feature extraction. Sparse-field methods are more robust against geometric transformations than dense-field methods. The performance of sparse-field methods may drop when detecting small or smooth copy-move forged regions. Although tremendous progress has been made in the field of conventional copy-move forgery detection methods, their hand-crafted features may not be optimal for downstream tasks, and there are many heuristics or manually

tuned thresholds [4], which may limit their performance. Thus, deep learning based copy-move forgery detection has drawn more attention recently, and some representative works are discussed in Section I [4]–[7].

### B. Transformer-Style Networks

Convolutional Neural Networks (CNNs) have been the mainstream in computer vision and other downstream tasks for years [1], [7]. Inspired by the major successes in natural language processing, Transformers [34] are adopted into the computer vision community. As the pioneer work, ViT [35] splits the input image into sequences of image patches, and builds pure Transformer blocks for image classification. ViT is also adopted for dense field prediction, e.g., SETR adopts ViT to extract features for semantic segmentation and incorporates a CNN decoder [36]. ViT has two inevitable limitations: single-scale low-resolution feature maps and high computational complexity for large images. Thus, researchers proposed different solutions to address these limitations. Wang et al. [9] extended ViT with pyramid structures named as Pyramid Vision Transformer (PVT). Liu et al. [8] proposed a hierarchical Transformer, i.e., Swin Transformer, whose representation is computed with shifted windows. Xie et al. [20] presented a hierarchically structured Transformer encoder without positional encoding, and a lightweight multi-layer MLP decoder. Transformers have been adopted for various downstream tasks, e.g., object detection [37], semantic segmentation [38], object tracking [39], super-resolution [40], object re-identification [41], and splicing detection [2], [24]. The application of Transformer for copy-move forgery detection still needs further research.

### C. MLP-Style Networks

In MLP-style networks, almost all network parameters are learned from MLP, and these networks can achieve comparable performance. MLP-Mixer [11] shows that neither convolution nor attention is necessary, the pure combination of MLPs applied independently to image patches and MLPs applied across patches can achieve promising results. Subsequently, Res-MLP [13] is constructed with residual MLP, gMLP [12] is designed based solely on MLPs with gating, S<sup>2</sup>-MLP [42] uses spatial-shift MLP for feature exchange, ViP [43] builds a Permute-MLP layer for spatial information encoding to capture long-range dependencies. AS-MLP [44] pays more attention to capture local dependencies by axially shifting channels of feature maps. CycleMLP [19] utilizes the Cycle Fully-Connected Layer (Cycle FC) which has linear complexity the same as channel FC and a larger receptive field than Channel FC. Their experimental results indicate an interesting issue that an attention-free architecture can also serve as a general vision backbone. In this paper, we verify the applicability of the MLP-style network on copy-move forgery detection.

### D. Continual Learning

Continual learning is also referred to as lifelong learning, sequential learning, and incremental learning [45]. The starting point of continual learning which is also the core of

continual learning is to learn without catastrophic forgetting: performance on a previously learned task or domain should not significantly degrade as new tasks or domains are added [15]. According to how task specific information is stored and used throughout the learning process, continual learning methods can be broadly divided into three categories: replay methods, regularization-based methods, parameter isolation methods. Replay methods store previous task samples or generate pseudo-samples, and replay these samples while learning a new task to alleviate forgetting [46]–[48]. Regularization-based methods introduce an extra regularization term in the loss function, maintaining previous knowledge when learning new tasks [14], [49]. Parameter isolation methods dedicate different model parameters to each task, to prevent any possible forgetting [50], [51]. Besides image classification, continual learning is adopted for numerous downstream tasks, e.g., object detection [52]–[54], semantic segmentation [55]–[57], instance segmentation [58]. Copy-move forgery detection aiming for pixel-level binary classification also faces a severe domain shift problem when handling different tasks. We attempt to alleviate this problem by continual learning.

## III. METHODOLOGY

In this paper, we propose CMFDFormer for copy-move forgery detection and a PCSDFramework. As shown in Fig. 1, CMFDFormer mainly consists of a backbone feature extractor, i.e., MiT, and a mask prediction network, i.e., PHD. In section III-A, MiT is introduced, and in section III-B, PHD is presented. In section III-C, we introduce our PCSDFramework.

### A. Mix Transformer Encoder

Copy-move forgery detection tries to compare all pairs of regions in one image, and find suspected duplicated regions. The basic computation procedure in self attention of Transformer is affinity matrix computation using key-query multiplication. The affinity matrix computation procedures are accumulated layer by layer which may be helpful to find visual similar regions. Mix Transformer (MiT) is a kind of Transformer network [20] which can provide multi-scale hierarchical feature maps. As shown in Fig. 1, MiT is built based on a hierarchical architecture with four Transformer modules and four corresponding output feature maps. Each Transformer module is composed of an overlap patch merging layer and several Transformer blocks. Each Transformer block is constituted by efficient multi-head self-attention and positional-encoding-free Mix-FFN (Feed-Forward Network).

1) *Hierarchical Architecture*: MiT constructs a hierarchical architecture which can generate multi-level multi-scale features. These features contain both high-resolution low-order features and low-resolution high-order features. Specifically, with an  $H \times W \times 3$  input image, we can generate a feature map  $\mathbf{F}_i$  with a resolution of  $\frac{H}{2^{i+1}} \times \frac{W}{2^{i+1}} \times C_i$ , and  $i \in \{1, 2, 3, 4\}$ . Each feature map is output by a Transformer module.

2) *Overlap Patch Merging*: Overlap patch merging is designed to preserve the local continuity around splitted patches, and it gradually degrades the resolution of feature maps. In

another word, the adjacent patches have overlapped regions which can avoid information fragmentation caused by non-overlap patch splitting. Let  $K$  denote the patch size,  $S$  denote the stride between two adjacent patches, and  $P_a$  denote the padding size. MiT sets  $K = 7, S = 4, P_a = 3$  in “Transformer module 1”, and sets  $K = 3, S = 2, P_a = 1$  in “Transformer module 2 – 4” to perform overlap patch merging which can be implemented by convolution operations.

3) *Efficient Multi-head Self-attention*: The large spatial scales of query, key and value in multi-head self-attention can increase computational burden of Transformer-style networks. Efficient multi-head self-attention reduces the spatial scale of key and value before the attention operation. The efficient multi-head self-attention in the  $j$ th stage is formulated as:

$$f_{\text{ems}}(\mathbf{Q}_j, \mathbf{K}_j, \mathbf{V}_j) = \cup(\text{head}_1, \dots, \text{head}_{N_j}) \mathbf{W}_j^O \quad (1)$$

$$\text{head}_{n_j} = \text{Atten}(\mathbf{Q}_j \mathbf{W}_{n_j}^Q, f_{sr}(\mathbf{K}_j) \mathbf{W}_{n_j}^K, f_{sr}(\mathbf{V}_j) \mathbf{W}_{n_j}^V) \quad (2)$$

where  $\mathbf{Q}_j, \mathbf{K}_j, \mathbf{V}_j$  are the input query, key and value at the  $j$ th stage (i.e., the  $j$ th Transformer block),  $\cup(\dots)$  denotes the concatenation operation along the channel dimension,  $\mathbf{W}_j^O \in \mathbb{R}^{C_j \times C_j}$ ,  $\mathbf{W}_{n_j}^Q \in \mathbb{R}^{C_j \times d_j}$ ,  $\mathbf{W}_{n_j}^K \in \mathbb{R}^{C_j \times d_j}$  and  $\mathbf{W}_{n_j}^V \in \mathbb{R}^{C_j \times d_j}$  are parameters of linear transformation.  $C_j$  denotes the channel of feature maps at the  $j$ th stage,  $N_j$  is the head number of the attention layer,  $n_j$  is the corresponding head index, the dimension of each head is  $d_j = \frac{C_j}{N_j}$ . The spatial reduction is computed as:

$$f_{sr}(\mathbf{x}) = \text{Norm}(\text{Reshape}(\mathbf{x}, R_j) \mathbf{W}_j^S) \quad (3)$$

where  $\mathbf{x} \in \mathbb{R}^{(h_j \times w_j) \times C_j}$  is the input sequence,  $R_j$  denotes the reduction ratio of the attention layers at stage  $j$ . The function  $\text{Reshape}(\mathbf{x}, R_j)$  reshapes  $\mathbf{x}$  to the size of  $\frac{h_j \times w_j}{R_j} \times (R_j \times C_j)$ , and  $\mathbf{W}_j^S \in \mathbb{R}^{(R_j \times C_j) \times C_j}$  is a linear projection which reduces  $\mathbf{x}$  to the dimension of  $C_j$ ,  $\text{Norm}(\cdot)$  denotes layer normalization. With transformed query  $\mathbf{q}_{n_j} \in \mathbb{R}^{(h_j \times w_j) \times d_j}$ , key  $\mathbf{k}_{n_j} \in \mathbb{R}^{\frac{h_j \times w_j}{R_j} \times d_j}$ , value  $\mathbf{v}_{n_j} \in \mathbb{R}^{\frac{h_j \times w_j}{R_j} \times d_j}$  at hands, the self-attention can be computed as:

$$\text{Atten}(\mathbf{q}_{n_j}, \mathbf{k}_{n_j}, \mathbf{v}_{n_j}) = \text{Softmax}\left(\frac{\mathbf{q}_{n_j} \mathbf{k}_{n_j}^T}{\sqrt{d_j}}\right) \mathbf{v}_{n_j} \quad (4)$$

4) *Positional-Encoding-Free Design*: MiT provides a kind of positional-encoding-free design by introducing Mix-FFN in which the effect of zero padding is considered to leak location information by directly using a  $3 \times 3$  convolution operation in the feed-forward network (FFN). Mix-FFN is computed as:

$$\mathbf{x}_{out} = \text{MLP}(\text{GELU}(\text{Conv}_{3 \times 3}(\text{MLP}(\mathbf{x}_{in})))) + \mathbf{x}_{in} \quad (5)$$

where  $\mathbf{x}_{in}$  is the feature map from efficient multi-head self-attention,  $\text{MLP}(\cdot)$  denotes channel-wise multi-layer perceptron,  $\text{GELU}(\cdot)$  is the GELU (Gaussian Error Linear Unit) activation function.

## B. Pluggable Hybrid Decoder

With multi-scale hierarchical features  $\mathbf{F}_i$  ( $i = 1, 2, 3, 4$ ) extracted by the backbone feature extractor at hand, we propose a Pluggable Hybrid Decoder (PHD) network to find matched

features and reconstruct suspected regions. “Pluggable” means our PHD can be assembled with different backbones, and “Hybrid” means PHD integrates multiple architectures with different flavors. As shown in Fig. 1, four groups of feature maps are passed through self-correlation computation to compute correlation maps; then, Feature Pyramid Network (FPN) [59] and Pyramid Pooling Module (PPM) [60] are constructed for hierarchical feature integration to get a concatenated tensor  $\bar{\mathbf{C}}$  with rich hierarchical information;  $\bar{\mathbf{C}}$  is further passed through a multi-scale Cycle fully-connected block for further multi-scale information investigation; finally, a mask reconstruction block is constructed to get the predicted mask.

1) *Self-correlation Computation*:  $\mathbf{F}_2, \mathbf{F}_3, \mathbf{F}_4$  are computed under the same self-correlation computation procedure.  $\mathbf{F}_1$  is input for self-correlation computation after being down-sampled by an overlap patch merging layer with  $K = 3, S = 2, P_a = 1$  for the tradeoff between memory costs and the localization performance. The self-correlation computation procedure aims to compute the similarity between every two locations in the feature maps. Firstly, L2 normalization is conducted at each location  $m$  of  $\mathbf{F}_i$ :

$$\bar{\mathbf{F}}_{i(m)} = f_{L2}(\mathbf{F}_{i(m)}) = \frac{\mathbf{F}_{i(m)}}{\|\mathbf{F}_{i(m)}\|_2} \quad (6)$$

where  $\|\cdot\|_2$  denotes L2 norm. Then, the scalar product is computed among every pair of locations:

$$\mathbf{C}_{i(m,n)} = (\bar{\mathbf{F}}_{i(m)})^T \bar{\mathbf{F}}_{i(n)} \quad (7)$$

by accumulating the computed results, we can get the correlation map  $\mathbf{C}_i = \{\mathbf{C}_{i(m,n)}\} \in \mathbb{R}^{(h_i \times w_i) \times (h_i \times w_i)}$ . In this paper, we use subscripts with brackets to index the feature map. In fact, a subset of  $\mathbf{C}_i$  contains sufficient information to decide which feature is matched, while the majority of scores in  $\mathbf{C}_i$  are weak-correlated.  $\mathbf{C}_i$  is reshaped to the scale of  $h_i \times w_i \times (h_i \times w_i)$ , and is sorted along the  $(h_i \times w_i)$  channels, and top- $T$  values are selected:

$$\tilde{\mathbf{C}}_{i(m,n,1:T)} = \text{Top}_T(\text{Sort}(\mathbf{C}_{i(m,n,:)})) \quad (8)$$

A monotonic decreasing curve with an abrupt drop at some point should be observed along the  $T$  channels, as long as  $\tilde{\mathbf{C}}_{i(m,n)}$  is matched and a proper  $T$  is selected. Zero-out and normalization operations are conducted on  $\tilde{\mathbf{C}}_i$  to limit correlation values to certain ranges and filter redundant values:

$$\bar{\mathbf{C}}_i = f_{L2}(\text{Max}(\tilde{\mathbf{C}}_i, 0)) \quad (9)$$

2) *Hierarchical Feature Integration*: After self-correlation computation, we can get a set of correlation maps  $\bar{\mathbf{C}}_i$  ( $i = 1, 2, 3, 4$ ) with different scales at different levels. How to integrate these correlation maps becomes a key problem. Here we adopt FPN [59] and PPM [60] for hierarchical multi-scale information investigation. As shown in Fig. 1,  $\bar{\mathbf{C}}_1, \bar{\mathbf{C}}_2, \bar{\mathbf{C}}_3$  are respectively recalibrated by  $1 \times 1$  convolution operations.  $\bar{\mathbf{C}}_4$  is recalibrated by a PPM module. In the PPM module, four parallel average pooling operations are conducted on  $\bar{\mathbf{C}}_4$  with pooling scales as  $\{1, 2, 3, 6\}$ , and four parallel  $1 \times 1$  convolution operations are followed. Then, the computed four sets of feature maps in PPM are resized to the same size as

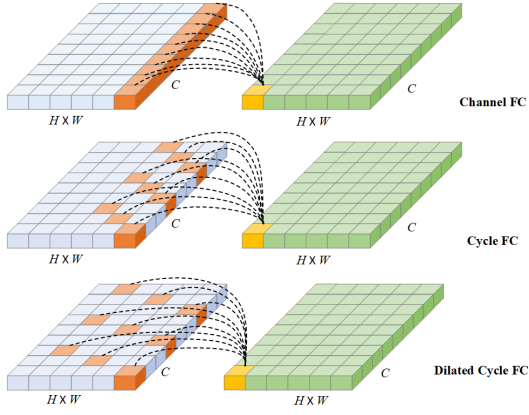


Fig. 2. Channel FC, Cycle FC ( $S_H \times S_W$  of  $3 \times 1$  with the dilation rate as 1) and dilated Cycle FC ( $S_H \times S_W$  of  $3 \times 1$  with the dilation rate as 2).

$\tilde{C}_4$ , and integrated by a  $3 \times 3$  convolutional layer.

Let  $C'_i$  denote the recalibrated correlation maps, low-level features are further integrated with high-level features by sequential upsampling operations  $f_{\times 2}$ , i.e.,  $C''_3 = C'_3 + f_{\times 2}(C'_4)$ ,  $C''_2 = C'_2 + f_{\times 2}(C''_3)$ ,  $C''_1 = C'_1 + C''_2$ . Then,  $C''_1, C''_2, C''_3$  are further processed by  $3 \times 3$  convolution operations respectively and resized to the same size as  $C''_1$ .  $C'_4$  is also resized to the same size as  $C''_1$ . All the resized feature maps are concatenated to a tensor  $\hat{C}$  which contains rich hierarchical information.

3) *Multi-Scale Cycle Fully-Connected Block*: Cycle Fully-Connected layer (Cycle FC) is proposed in CycleMLP [19] to introduce larger receptive fields for MLP. As shown in Fig. 2, Channel FC which is commonly seen in MLP-like networks applies a weighting matrix along the channel dimension on a fixed position  $(m, n)$ , while Cycle FC introduces a receptive field of  $(S_H, S_W)$ ,  $S_H$  is the stepsize along with the height dimension,  $S_W$  is the stepsize along with the width dimension. In Fig. 2, we show a simple example of Cycle FC whose  $S_H$  is 3 and  $S_W$  is 1. In the previous step, we can get the concatenated feature map  $\hat{C} \in \mathbb{R}^{H_c \times W_c \times C_{in}}$ , where  $H_c = H/8$  and  $W_c = W/8$ . The Cycle FC operator can be formulated as below:

$$\text{CycleFC}(\hat{C})_{(m,n,:)} = \sum_{c=0}^{C_{in}} \hat{C}_{(m+\delta_m(c), n+\delta_n(c), c)} \cdot \mathbf{W}_{(c,:)}^{mlp} + \mathbf{b} \quad (10)$$

where  $\mathbf{W}^{mlp} \in \mathbb{R}^{C_{in} \times C_{out}}$  and  $\mathbf{b} \in \mathbb{R}^{C_{out}}$  are parameters of Cycle FC.  $\delta_m(c)$  and  $\delta_n(c)$  are the spatial offset values of the two axes on the  $c$ th channel, which are defined as below:

$$\delta_m(c) = (c \bmod S_H) - 1 \quad (11)$$

$$\delta_n(c) = (\lfloor \frac{c}{S_H} \rfloor \bmod S_W) - 1 \quad (12)$$

Making use of Cycle FC, we design a multi-scale Cycle FC block. The receptive field of Cycle FC can be enlarged by setting a larger dilation rate with a small kernel. As shown in Fig. 2, a small kernel  $S_H \times S_W$  of  $3 \times 1$  with the dilation rate as 2 has an obviously larger receptive field along  $H \times W$ . Multi-scale Cycle FC block consists of nine parallel multi-scale Cycle FCs, which have stepsizes  $S_H \times S_W$

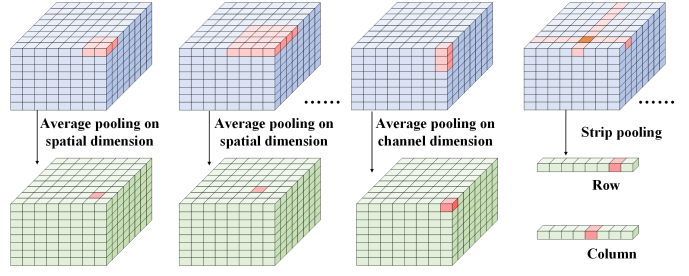


Fig. 3. Cube pooling and strip pooling in PCSD.

of  $1 \times 3$  (four  $1 \times 3$  Cycle FCs with dilation rates as  $\{1, 6, 12, 18\}$ ),  $3 \times 1$  (four  $3 \times 1$  Cycle FCs with dilation rates as  $\{1, 6, 12, 18\}$ ), and  $1 \times 1$ . These Cycle FCs are denoted as  $\{\text{CycleFC}_r(\hat{C}) | r = 1, 2, \dots, 9\}$ . And the multi-scale Cycle FC block can be formulated as:

$$\tilde{C} = \text{Conv}_{3 \times 3}(\hat{C} + f_{linear}(\sum_{r=1}^9 \beta_r \text{CycleFC}_r(\hat{C}))) \quad (13)$$

where  $\beta_r$  is a learnable parameter,  $f_{linear}$  is a channel-wise linear transform, and  $\tilde{C}$  is the output correlation map reinforced by multi-scale Cycle FC.  $\text{Conv}_{3 \times 3}$  denotes a  $3 \times 3$  convolution operation followed by a ReLU function.

4) *Mask Reconstruction*: In order to reconstruct the final predicted mask from  $\tilde{C}$ , we construct a simple mask reconstruction network:

$$\mathbf{M} = f_{convseg}(f_{upscale}(\tilde{C})) \quad (14)$$

$$f_{upscale}(\tilde{C}) = \text{Conv}_{1 \times 1}(f_{\times 2}(\text{Conv}_{1 \times 1}(f_{\times 2}(\text{Conv}_{1 \times 1}(f_{\times 2}(\tilde{C})))))) \quad (15)$$

where  $\mathbf{M} \in \mathbb{R}^{H \times W \times 2}$  is the predicted mask,  $f_{convseg}$  is a  $1 \times 1$  convolutional layer with softmax,  $f_{upscale}$  consists of three  $1 \times 1$  convolutional layers  $\text{Conv}_{1 \times 1}$  and three bilinear upsampling layers  $f_{\times 2}$ .  $\text{Conv}_{1 \times 1}$  is followed by an activation function of ReLU.

### C. PCSD Continual Learning

Deep learning based copy-move forgery detection faces the performance drop when processing new data which has different distributions with the training data. We propose a PCSD continual learning framework for CMFDFormer to keep comparable performance on both new data and former data. In continual learning, a distillation loss is commonly formulated between the predictions of the previous and current models to alleviate catastrophic forgetting. The pooling operation plays a key role in designing the distillation loss to transfer knowledge. We design a PCSD loss which integrates cube pooling and strip pooling [17], [61], to capture information from both square regions and long-range banded regions. As shown in Fig. 3, the cube pooling mainly contains multi-scale average pooling on the spatial dimension and average pooling on the channel dimension, and strip pooling conducts long narrow pooling along the row and column. Besides, continual learning methods based on knowledge distillation in other computer vision tasks often adopt intermediate features from feature

extractors for knowledge distillation. The same setting in the copy-move forgery detection network is difficult to converge. In our PCSO continual learning, we leverage the predicted mask and the feature maps of intermediate layers after self-correlation computation in PHD for knowledge distillation.

The predicted mask and PHD intermediate feature maps  $\{\mathbf{X}^k | k = 1, \dots, 6\} = \{\mathbf{M}, \tilde{\mathbf{C}}, \mathbf{C}'_1, \mathbf{C}'_2, \mathbf{C}'_3, \mathbf{C}'_4\}$  are selected for distillation. Let  $K$  denote the total number of distilled feature maps  $\{\mathbf{X}^k\}$ , and  $K = 6$  in our formulation.  $\mathbf{M}$  is the predicted mask,  $\tilde{\mathbf{C}}$  is the output feature map of multi-scale Cycle FC block in Eq. (13),  $\{\mathbf{C}'_i\}$  are the recalibrated correlation maps in the hierarchical feature integration module. We conduct cube pooling on  $\mathbf{X}^k$ , i.e., multi-scale average pooling on the spatial dimension and average pooling on the channel dimension. The pooled feature  $\tilde{\mathbf{X}}^{T,k,p}$ ,  $\tilde{\mathbf{X}}^{S,k,p}$  of the teacher model and the student model can be calculated by the average pooling operation  $\odot$ :

$$\tilde{\mathbf{X}}^{T,k,p} = \mathbf{P}_p \odot \mathbf{X}^{T,k} \quad (16)$$

$$\tilde{\mathbf{X}}^{S,k,p} = \mathbf{P}_p \odot \mathbf{X}^{S,k} \quad (17)$$

where  $\mathbf{P}_p$  denotes the  $p$ th average pooling kernel, the stride is set to 1, the superscript  $T$  indicates the teacher model, and  $S$  indicates the student model. For multi-scale average pooling on the spatial dimension, the size of kernel  $\mathbf{P}_p$  belongs to  $\mathcal{P}_s = \{4, 8, 12, 16, 20, 24\}$ . For average pooling on the channel dimension,  $\mathcal{P}_c = \{3\}$ . The knowledge distillation loss of cube pooling can be formulated as follows:

$$\mathcal{L}_{cpkd} = \frac{1}{K} \frac{1}{P} \sum_{k=1}^K \sum_{p=1}^P \|\tilde{\mathbf{X}}^{T,k,p} - \tilde{\mathbf{X}}^{S,k,p}\|_2 \quad (18)$$

where  $P = |\mathcal{P}_s| + |\mathcal{P}_c|$  denotes the number of average pooling kernels.

Multi-scale average pooling on the spatial domain belongs to conventional spatial pooling which has a square shape, and it probes the input feature maps within square windows which limit their flexibility in capturing anisotropy context. Especially, in copy-move forgeries, the duplicated regions may distribute discretely or have a long-range banded structure. Although the large square pooling window can contain long-range information, it inevitably incorporates contaminating information from irrelevant regions. Strip pooling considers a long but narrow kernel, and can capture long-range information with less contaminating information.

We adopt a multi-scale strip pooling architecture which divides the input feature map  $\mathbf{X}^k$  into multi-scale blocks and conduct strip pooling on each block. The feature maps after multi-scale strip pooling can be formulated as:

$$\tilde{\mathbf{X}}^{T,k} = \cup(\{\Psi^q(\mathbf{X}^{T,k})\}) \quad (19)$$

$$\tilde{\mathbf{X}}^{S,k} = \cup(\{\Psi^q(\mathbf{X}^{S,k})\}) \quad (20)$$

where  $\cup(\dots)$  denotes the concatenation operation along the channel dimension, and  $q = 1, \dots, Q$  denotes how many blocks we divide, e.g., there is only  $1^2$  block when  $q = 1$ , there are  $2^2$  blocks when  $q = 2$ . In our implementation,  $Q = 2$  for  $k = 2, \dots, 6$ ;  $Q = 4$  for  $k = 1$ , i.e.,  $q = 1, 2, 3, 4$  for  $\mathbf{M}$ .

The  $q$ th strip pooled feature map can be formulated as:

$$\Psi^q(\mathbf{X}^k) = \sqcup(\Phi(\mathbf{X}^{k,0,0}), \dots, \Phi(\mathbf{X}^{k,q-1,q-1})) \quad (21)$$

where  $\mathbf{X}^{k,m,n} = \mathbf{X}^k_{(mH_k/q:(m+1)H_k/q, nW_k/q:(n+1)W_k/q, :)}$  is a sub-region of  $\mathbf{X}^k$  with the scale as  $\frac{H_k}{q} \times \frac{W_k}{q} \times C_k$ ,  $\forall m = 0, \dots, q-1, \forall n = 0, \dots, q-1$ .  $\sqcup(\dots)$  denotes concatenation over the channel axis, e.g.,  $\Psi^q(\mathbf{X}^k) \in \mathbb{R}^{(H_k+W_k) \times q \times C_k}$ ,  $\Phi(\mathbf{X}^{k,m,n}) \in \mathbb{R}^{(\frac{H_k}{q} + \frac{W_k}{q}) \times C_k}$ . The embedded feature of the  $(m, n)$  block can be computed as:

$$\Phi(\mathbf{X}^{k,m,n}) = \sqcup(\mathbf{Q}_w \odot \mathbf{X}^{k,m,n}, \mathbf{Q}_h \odot \mathbf{X}^{k,m,n}) \quad (22)$$

where  $\mathbf{Q}_w$  denotes the width-pooled kernel and  $\mathbf{Q}_h$  denotes the height-pooled kernel. The knowledge distillation loss of strip pooling can be formulated as follows:

$$\mathcal{L}_{spkd} = \frac{1}{K} \sum_{k=1}^K \|\tilde{\mathbf{X}}^{T,k} - \tilde{\mathbf{X}}^{S,k}\|_2 \quad (23)$$

Thus, the final loss in the pooled cube and strip distillation stage is formulated as follows:

$$\mathcal{L} = \mathcal{L}_{ce} + \lambda(\mathcal{L}_{cpkd} + \mathcal{L}_{spkd}) \quad (24)$$

where  $\lambda$  is the hyper parameter of distillation loss weight, and  $\mathcal{L}_{ce}$  is the cross-entropy loss:

$$\mathcal{L}_{ce} = \sum_{m=1}^H \sum_{n=1}^W \sum_{c=1}^{C_M} \mathbf{G}_{(m,n,c)} \log(\mathbf{M}_{(m,n,c)}) \quad (25)$$

where  $\mathbf{G}_{(m,n,c)}$  denotes the ground-truth value at position  $(m, n, c)$ ,  $\mathbf{M}_{(m,n,c)}$  denotes the predicted value at  $(m, n, c)$ ,  $C_M$  denotes the channel number of the predicted mask.

## IV. EXPERIMENTAL EVALUATION

In this section, we first introduce the training and evaluation details in section IV-A, then ablation study is conducted in section IV-B to select an appropriate network architecture and a continual learning scheme, and the proposed framework is compared with the state-of-the-art methods in section IV-C.

### A. Training and Evaluation Details

The proposed network, training/continual learning/testing scripts and all compared backbones are implemented based on MMsegmentation<sup>1</sup>. All the backbone networks are initialized by parameters pretrained on ImageNet<sup>2</sup>. As for the ablation study of continual learning, we mainly adopt two synthetic copy-move forgery datasets, i.e., USCISI [4], and BESTI<sup>3</sup> [7], which have sufficient training images. USCISI has 80,000 training images, 10,000 validation images and 10,000 testing images. BESTI has 120,000 training images and 1,000 testing images. In order to demonstrate the effectiveness of our continual learning framework with unbalanced pretraining and continual learning datasets, we split three publicly available datasets:

<sup>1</sup><https://mmsegmentation.readthedocs.io/en/latest/>

<sup>2</sup><https://www.image-net.org/>

<sup>3</sup><https://github.com/yaqiliu-cs/SelfDM-TIP>



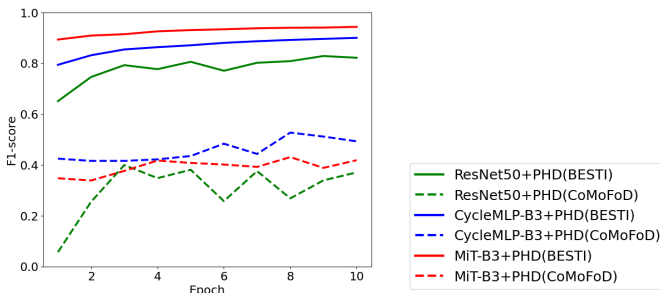
- **CoMoFoD**: There are 200 base forged images and 24 other categories which are made by applying postprocessing/attacks to the base forged images to hide forgery clues. We randomly divide the base forged images into two groups: CoMoFoD-subset1 with 100 base forged images and 24 other categories (total 2,500 images) for training, CoMoFoD-subset2 with other 100 base forged images and 24 categories for testing.
- **CASIA**: There are 1,313 copy-move forged images in total. We randomly divide it into two groups: 1,000 images for training (CASIA-subset1), and 313 images for testing (CASIA-subset2).
- **COVERAGE**: It is designed to address tamper detection ambiguity caused by self-similarity within natural images [62]. COVERAGE contains 100 original images which have similar-but-genuine objects, and corresponding 100 copy-move forged images. Discarding 10 mismatched image and ground truth mask pairs, we randomly select 65 forged images and corresponding original images for training (COVERAGE-subset1), 25 forged images for evaluating the pixel-level F1-score (COVERAGE-subset2), and 25 original images for testing the image-level false alarm rate (FAR) (COVERAGE-subset3).

As for the evaluation metrics, we compute the pixel-level F1-score of each image, and compute their average F1-score of all evaluated images in the testing dataset. Since there is no ground-truth mask for original images in COVERAGE-subset3, we compute the image-level FAR.

## B. Ablation Study

TABLE I  
BACKBONE AND PHD STEP-BY-STEP F1-SCORE ANALYSES ON BESTI.

Decoder \ Encoder	Encoder		
	ResNet50	CycleMLP-B3	MiT-B3
MR	0.646	0.895	0.939
MR+HFI	0.807	0.898	0.945
PHD (MR+HFI+MSCFC)	0.863	0.910	0.951



	ResNet50+PHD	CycleMLP-B3+PHD	MiT-B3+PHD
FLOPs	143.43G	56.77G	50.78G
Params	49.23M	58.43M	64.63M

Fig. 4. F1-score and model efficiency of ResNet50+PHD, CycleMLP-B3+PHD, MiT-B3+PHD on BESTI testing images and CoMoFoD subset2.

TABLE II  
PCSD CONTINUAL LEARNING ANALYSES ON THE SYNTHETIC DATASETS.

Variant	Train dataset	CL dataset	Test dataset	F1-score
ResNet50 + PHD	USCISI	-	USCISI	0.698
	USCISI	-	BESTI	0.518
	BESTI	-	USCISI	0.276
	BESTI	-	BESTI	0.863
	USCISI	BESTI	USCISI	0.630 (-0.068)
	USCISI	BESTI	BESTI	0.692 (+0.174)
	BESTI	USCISI	USCISI	0.576 (+0.300)
CycleMLP-B3 + PHD	BESTI	USCISI	BESTI	0.767 (-0.096)
	USCISI	-	USCISI	0.885
	USCISI	-	BESTI	0.541
	BESTI	-	USCISI	0.338
	BESTI	-	BESTI	0.910
	USCISI	BESTI	USCISI	0.678 (-0.207)
	USCISI	BESTI	BESTI	0.734 (+0.193)
MiT-B3 + PHD	BESTI	USCISI	USCISI	0.648 (+0.330)
	BESTI	USCISI	BESTI	0.852 (-0.058)
	USCISI	-	USCISI	0.944
	USCISI	-	BESTI	0.526
	BESTI	-	USCISI	0.420
	BESTI	-	BESTI	0.951
	USCISI	BESTI	USCISI	0.900 (-0.044)
USCISI	BESTI	BESTI	0.844 (+0.318)	
	BESTI	USCISI	USCISI	0.832 (+0.412)
	BESTI	USCISI	BESTI	0.924 (-0.027)

TABLE III  
MEAN F1-SCORE OF CMFD FORMER AFTER CONTINUAL LEARNING ON USCISI AND BESTI DATASETS.

Distillation method	USCISI→BESTI	BESTI→USCISI
	Mean F1-score	Mean F1-score
Strip pooling	0.868	0.875
Cube pooling	0.870	0.874
PCSD	0.872	0.878

1) *Backbone and PHD Analyses*: As shown in TABLE I, we adopt three different style backbones, i.e., ResNet50 (CNN-style), CycleMLP-B3 (MLP-style), and MiT-B3 (Transformer-style). As for PHD, there are three variants, i.e., “MR” which only has the mask reconstruction block with concatenated feature maps after self-correlation computation as the input, “HFI+MR” which adds the hierarchical feature integration module, and the final “PHD” which further adds the Multi-Scale Cycle FC (MSCFC) block. It can be clearly seen from TABLE I that MiT-B3 can achieve better performance than CycleMLP-B3, and CycleMLP-B3 can achieve higher scores than ResNet50. Besides, each component in PHD is helpful to improve the performance. Considering that “PHD” is fit for different backbones, which is why it is called “Pluggable”, we finally select “PHD” for the mask prediction. Besides, in Fig. 4, F1-scores along each epoch of the three variants on the BESTI testing set and CoMoFoD subset2 are provided. Ten-epoch training is conducted on the combined datasets of USCISI and BESTI. “MiT-B3+PHD” achieves the highest score on BESTI while its scores are lower than “CycleMLP-

B3+PHD” on CoMoFoD. It indicates that “MiT-B3+PHD” has better learning ability, and “CycleMLP-B3+PHD” has better generalization ability. Among the three compared variants, “MiT-B3+PHD” has more parameters with fewer FLOPs.

2) *Continual Learning Analyses*: PCSD continual learning framework is analysed from two aspects: PCSD continual learning on the synthetic datasets with three different backbones in TABLE II, and the strip/cube pooling evaluation in TABLE III.

In TABLE II, “Train dataset” denotes the dataset for training or pretraining, “CL dataset” denotes the dataset for continual learning, and “Test dataset” is the dataset for testing. For some variants, there is no “CL dataset”, and we use “-” to denote null. From TABLE II, we can see that there are clear score drops when the training dataset and the testing dataset are different, e.g., ResNet50 with a drop of 0.384  $((0.698 - 0.276 + 0.863 - 0.518)/2)$ , CycleMLP-B3 with 0.458, MiT-B3 with 0.475. In fact, the other state-of-the-art deep learning based copy-move forgery detection methods (e.g., CMSDNet, SelfDM-SA+PS+CRF) also face this poor generalization ability problem. With the help of PCSD continual learning, the three variants with different backbones can achieve comparable performance on both USCISI and BESTI. The MiT-B3 backbone can achieve the best performance, and all its F1-scores are higher than 0.8 after PCSD continual learning. Especially, the score decreases on former datasets are less than 0.05, and score increases on continual learning datasets are more than 0.30.

Difficult tradeoffs are made according to the experiments of TABLE I, TABLE II and Fig. 4. “MiT-B3+PHD” can achieve excellent performance with different training datasets, and its continual learning performance is even more excellent with less than 0.05 decrease and larger than 0.30 increase. Although “CycleMLP-B3+PHD” can achieve good performance on CoMoFoD with F1-score larger than 0.52, its learning ability on training datasets and its continual learning performance are worse than “MiT-B3+PHD”. Thus, we select “MiT-B3+PHD” as our final solution. In our view, powerful learning ability and stable continual learning are more important. When facing new tasks with sufficient training datasets and appropriate continual learning datasets, “MiT-B3+PHD” shows more promising performance. In the following, “MiT-B3+PHD” is written as “CMFDFormer”.

In TABLE III, we demonstrate the effectiveness of both strip pooling and cube pooling. “USCISI→BESTI” denotes that USCISI is used for pretraining and BESTI is used for continual learning. “BESTI→USCISI” denotes that BESTI is used for pretraining and USCISI is used for continual learning. We compute the average F1-scores on USCISI and BESTI after continual learning for comparison. The motivation of combining cube pooling and strip pooling is that the duplicated regions may distribute discretely or have long-range banded structures in copy-move forgeries. Multi-scale square pooling windows in cube pooling are critical to capturing multi-scale local features. When processing discretely distributed regions or long-range banded regions, large square pooling windows would inevitably incorporate contaminating information from irrelevant regions. Strip pooling considers a long but narrow

kernel, and can capture long-range information with less contaminating information. In fact, both strip pooling and cube pooling over our CMFDFormer’s continual learning framework can achieve comparable performance, while PCSD has better performance.

### C. Comparison with Other Methods

In this section, CMFDFormer is compared with three conventional copy-move forgery detection methods (LiJ [29], Cozzolino [26], LiY [3]) and three deep learning based copy-move forgery detection methods (BusterNet [4], CMSDNet [6], SelfDM-SA+PS+CRF [7]) on five datasets, i.e., USCISI, BESTI, CoMoFoD, CASIA, COVERAGE. All the scores are generated based on the released codes of the original papers.

TABLE IV  
COMPARISONS ON USCISI AND BESTI.

Method	USCISI F1-score	BESTI F1-score
LiJ	0.399	0.360
Cozzolino	0.169	0.273
LiY	0.210	0.395
BusterNet	0.464	0.421
CMSDNet	0.692	0.429
SelfDM-SA+PS+CRF	0.346	0.831
CMFDFormer	0.944	0.951

In TABLE IV, the F1-scores on USCISI and BESTI of compared methods are listed. Both USCISI and BESTI are synthetic datasets in which duplicated regions suffer from different transformations, e.g., rotation, scale, deformation changes. It is difficult for conventional methods to handle these changes, and these methods have lower scores than deep learning based methods. While deep learning based copy-move forgery detection methods are confronted with the robustness problem against the domain shift. Even both USCISI and BESTI have synthetic images generated from MS COCO [63] (USCISI is generated from MS COCO and MIT SUN2012 [64], BESTI is generated from MS COCO), CMSDNet which is trained on USCISI has clear score decreases on BESTI, and the score of SelfDM-SA+PS+CRF trained on BESTI also decreases on USCISI. CMFDFormer also faces this problem as we discussed in Section IV-B2. While CMFDFormer trained on a single training dataset can achieve the highest score on the corresponding testing set.

Both USCISI and BESTI have sufficient training images, while the training images are difficult to obtain in other tasks under the practical circumstances. The training subsets of CoMoFoD/CASIA/COVERAGE are much smaller than the training sets of USCISI and BESTI. With unbalanced pretraining datasets and continual learning datasets, the effectiveness of PCSD continual learning still needs to be verified. Besides, the proposed framework is also compared with the state-of-the-art deep learning based copy-move forgery detection methods with publicly available training codes, i.e., CMSDNet<sup>4</sup> which

<sup>4</sup><https://github.com/imagecbj/A-serial-image-copy-move-forgery-localization-scheme-with-source-target-distinguishment>



TABLE V  
F1-SCORE ANALYSES OF DEEP LEARNING BASED METHOD FINETUNING OR CONTINUAL LEARNING.

Method	Train dataset	Finetune/CL dataset	USCISI	BESTI	CoMoFoD-subset2	CASIA-subset2	COVERAGE-subset2
CMSDNet	USCISI	-	0.692		0.483	0.475	0.772
		CoMoFoD-subset1	0.193 (-0.499)		0.677 (+0.194)		
		CASIA-subset1	0.194 (-0.498)			0.555 (+0.080)	
		COVERAGE-subset1	0.331 (-0.361)				0.743 (-0.029)
SelfDM-SA +PS+CRF	BESTI	-		0.831	0.506	0.475	0.803
		CoMoFoD-subset1		0.495 (-0.336)	0.678 (+0.172)		
		CASIA-subset1		0.683 (-0.148)		0.606 (+0.131)	
		COVERAGE-subset1		0.731 (-0.100)			0.698 (-0.105)
CMFDFormer	USCISI +BESTI	-	0.941	0.944	0.419	0.316	0.526
		CoMoFoD-subset1	0.803 (-0.138)	0.856 (-0.088)	0.684 (+0.265)		
		CASIA-subset1	0.823 (-0.118)	0.845 (-0.099)		0.578 (+0.262)	
		COVERAGE-subset1	0.694 (-0.247)	0.808 (-0.136)			0.820 (+0.294)

TABLE VI  
COMPARISONS ON CoMoFoD SUBSET2, CASIA SUBSET2, COVERAGE SUBSET2 AND SUBSET3.

Method	CoMoFoD-subset2 F1-score	CASIA-subset2 F1-score	COVERAGE subset2 F1-score	COVERAGE-subset3 FAR
LiJ	0.437	0.052	0.712	0.760
Cozzolino	0.424	0.203	0.629	0.360
LiY	0.509	0.279	0.680	0.520
BusterNet	0.525	0.420	0.721	0.880
CMSDNet	0.483	0.475	0.772	1.000
SelfDM-SA+PS+CRF	0.506	0.475	0.803	0.960
CMFDFormer++	0.684	0.578	0.820	0.640

is trained on USCISI, and SelfDM-SA+PS+CRF<sup>5</sup> which is trained on BESTI. For fair comparison, we adopt the subsets of CoMoFoD/CASIA/COVERAGE to finetune the released pretrained CMSDNet and SelfDM-SA+PS+CRF models. As shown in TABLE V, simply finetuning can cause catastrophic forgetting. The score increases on finetuned datasets are even smaller than the score decreases on former datasets. Furthermore, it is even difficult to increase the score on COVERAGE by finetuning. To simultaneously compare with CMSDNet and SelfDM-SA+PS+CRF, both USCISI and BESTI are adopted as the pretraining datasets, and the subsets of CoMoFoD/CASIA/COVERAGE are respectively adopted for continual learning. After PCSD continual learning, the scores on the testing subsets can be dramatically improved, while the score decreases on USCISI and BESTI are acceptable. This experiment demonstrates that when we only have a small number of images for continual learning, our PCSD continual learning framework is still helpful. In the following, the models after continual learning are denoted as ‘‘CMFDFormer++’’.

In TABLE VI, the scores on the CoMoFoD-subset2, CASIA-subset2, and COVERAGE subset2/subset3 are provided. On CASIA-subset2, we find that deep learning based methods can achieve better performance than conventional methods. While on CoMoFoD-subset2 and COVERAGE-subset2, deep learning based methods have no obvious advantage than conventional methods. Especially, deep learning based methods have high false alarm rates on COVERAGE-subset3. CMFDFormer++ can achieve higher F1-scores on all

testing datasets, while it also has a high false alarm rate of 0.64 on COVERAGE-subset3. COVERAGE is designed to evaluate the ability of distinguishing copy-move forged regions and similar-but-genuine regions, and duplicated regions suffer copy-move forgeries without complicated transforms. Conventional methods can handle these cases well, while the robustness of deep learning based methods against different transforms cause that they are difficult to distinguish copy-move forged regions and similar-but-genuine regions. Fig. 5 further provides the F1-scores on the CoMoFoD-subset2 images under attacks, CMFDFormer++ shows good robustness against different attacks.

Visual comparisons on CoMoFoD-subset2 are provided in Fig. 6, six challenging examples are listed. The first three columns are large-area duplicated regions, and the last three columns are small duplicated objects. In the first three columns, we find conventional methods even can achieve better performance, especially Cozzolino can generate almost perfect results. The results of compared deep learning based methods are unsatisfied, while CMFDFormer++ can achieve good performance. In the last three columns, it is difficult for conventional methods to detect copy-move forged regions, and the detected regions of compared deep learning based methods are not accurate enough. While CMFDFormer++ can generate more accurate results.

In Fig. 7, visual comparisons on CASIA-subset2 and COVERAGE-subset2 are provided. The first four columns are examples from CASIA-subset2, and the last two columns are examples from COVERAGE-subset2. In the 1st column,

<sup>5</sup><https://github.com/yaqiliu-cs/SelfDM-TIP>

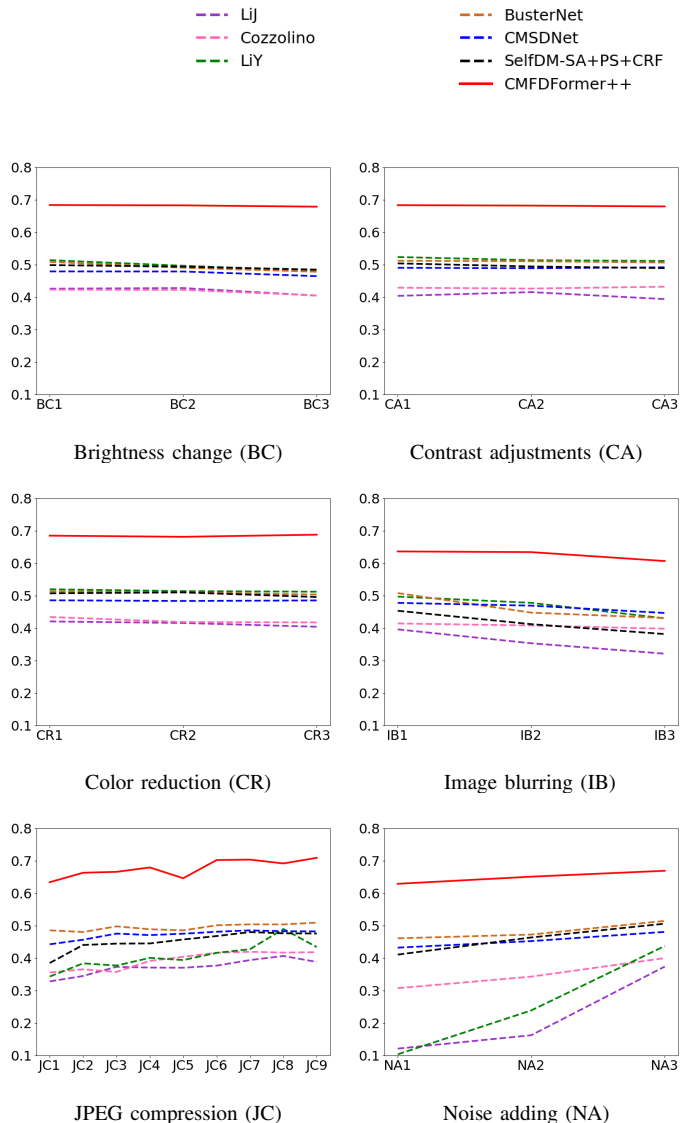


Fig. 5. F1-scores (y-axis) on CoMoFoD subset2 under attacks (x-axis).

conventional methods can not detect any suspected regions, while deep learning based methods can detect duplicated regions. CMSDNet detects many false-alarm regions. In the 2nd column, all methods can detect duplicated regions, while CMFDFormer++ is more accurate. In the 3rd and 4th columns, there are many disturbance terms in the backgrounds, there are even multiple duplicated pairs in the 4th column. We find that only CMFDFormer++ can detect meaningful regions. In the 5th column, we find that the compared deep learning based methods are difficult to detect intact and accurate regions, while the results of conventional methods and CMFDFormer++ have high quality. In the last column, there are many black tags which disturb the detection, and Cozzolino, LiY and CMFDFormer++ are more accurate.

## V. CONCLUSION

In this paper, we propose a Transformer-style copy-move forgery detection network named as CMFDFormer, and pro-

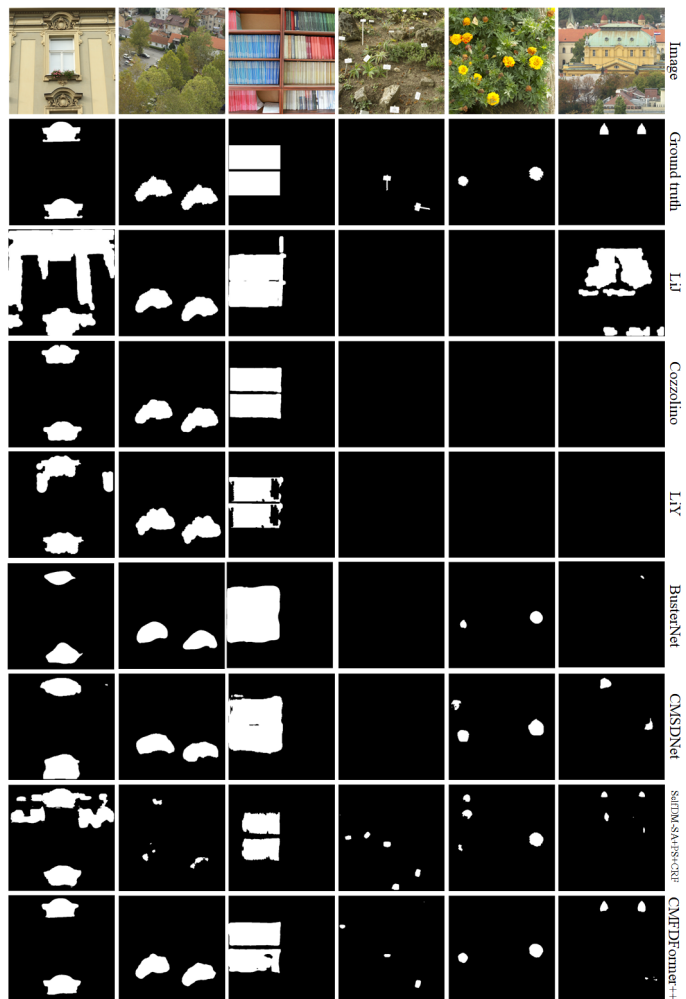


Fig. 6. Visual comparison on CoMoFoD-subset2.

pose a PCSD continual learning framework for CMFDFormer. CMFDFormer consists of a backbone feature extractor, i.e., MiT, and a mask prediction network, i.e., PHD. MiT is adopted based on comprehensive comparisons among Transformer-style, MLP-style and CNN-style networks. PHD is composed of self-correlation, hierarchical feature integration, a multi-scale Cycle fully-connected block and a mask reconstruction block. CMFDFormer can achieve excellent performance within the same synthetic dataset, however it is confronted with the performance drop problem caused by domain shift, which is also common in other deep learning based copy-move forgery detection methods. To alleviate this problem, we propose a novel PCSD continual learning framework. Instead of leveraging intermediate features of backbones, our continual learning framework integrates intermediate features of PHD. Our PCSD loss makes use of cube pooling and strip pooling to handle multi-scale information in square windows and information in long-range banded regions at the same time. Extensive experiments demonstrate the effectiveness of CMFDFormer and our PCSD continual learning framework.

In our work, we make a preliminary attempt in the field of continual learning for copy-move forgery detection. A possible solution is first put forward in the field of copy-move forgery

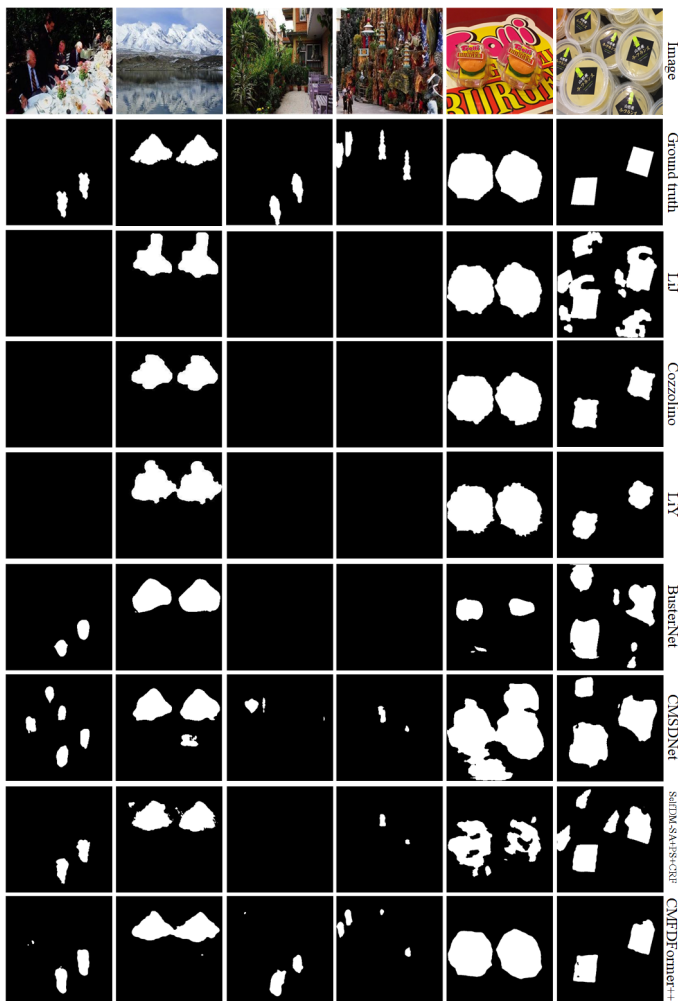


Fig. 7. Visual comparison on CASIA-subset2 and COVERAGE-subset2.

detection: a powerful copy-move forgery detection network which can handle numerous cases may be difficult to get at once, while it can be gradually raised by continual learning when facing new cases. In the future, there are still two main issues which need to be concerned: robust backbones should be thoroughly investigated to balance generalization ability and learning ability; customized continual learning models for copy-move forgery detection should be thoroughly studied with fewer performance drops on former data and better performance on new data.

## REFERENCES

- [1] Y. Liu, X. Zhu, X. Zhao, and Y. Cao, "Adversarial learning for constrained image splicing detection and localization based on atrous convolution," *IEEE Transactions on Information Forensics and Security*, vol. 14, no. 10, pp. 2551–2566, 2019.
- [2] Y. Liu, B. Lv, X. Jin, X. Chen, and X. Zhang, "Tbformer: Two-branch transformer for image forgery localization," *IEEE Signal Processing Letters*, vol. 30, pp. 623–627, 2023.
- [3] Y. Li and J. Zhou, "Fast and effective image copy-move forgery detection via hierarchical feature point matching," *IEEE Transactions on Information Forensics and Security*, vol. 14, no. 5, pp. 1307–1322, 2019.
- [4] Y. Wu, W. Abd-Almageed, and P. Natarajan, "Busternet: Detecting copy-move image forgery with source/target localization," in *Proceedings of the European Conference on Computer Vision (ECCV)*, 2018, pp. 168–184.
- [5] J.-L. Zhong and C.-M. Pun, "An end-to-end dense-inceptionnet for image copy-move forgery detection," *IEEE Transactions on Information Forensics and Security*, vol. 15, pp. 2134–2146, 2020.
- [6] B. Chen, W. Tan, G. Coatrieux, Y. Zheng, and Y. Q. Shi, "A serial image copy-move forgery localization scheme with source/target distinguishment," *IEEE Transactions on Multimedia*, 2020.
- [7] Y. Liu, C. Xia, X. Zhu, and S. Xu, "Two-stage copy-move forgery detection with self deep matching and proposal superglue," *IEEE Transactions on Image Processing*, vol. 31, pp. 541–555, 2022.
- [8] Z. Liu, Y. Lin, Y. Cao, H. Hu, Y. Wei, Z. Zhang, S. Lin, and B. Guo, "Swin transformer: Hierarchical vision transformer using shifted windows," in *Proceedings of the IEEE/CVF international conference on computer vision*, 2021, pp. 10 012–10 022.
- [9] W. Wang, E. Xie, X. Li, D.-P. Fan, K. Song, D. Liang, T. Lu, P. Luo, and L. Shao, "Pyramid vision transformer: A versatile backbone for dense prediction without convolutions," in *Proceedings of the IEEE/CVF international conference on computer vision*, 2021, pp. 568–578.
- [10] —, "Pvt v2: Improved baselines with pyramid vision transformer," *Computational Visual Media*, vol. 8, no. 3, pp. 415–424, 2022.
- [11] I. O. Tolstikhin, N. Houlsby, A. Kolesnikov, L. Beyer, X. Zhai, T. Unterthiner, J. Yung, A. Steiner, D. Keysers, J. Uszkoreit et al., "Mlp-mixer: An all-mlp architecture for vision," *Advances in neural information processing systems*, vol. 34, pp. 24 261–24 272, 2021.
- [12] H. Liu, Z. Dai, D. So, and Q. V. Le, "Pay attention to mlps," *Advances in Neural Information Processing Systems*, vol. 34, pp. 9204–9215, 2021.
- [13] H. Touvron, P. Bojanowski, M. Caron, M. Cord, A. El-Nouby, E. Grave, G. Izacard, A. Joulin, G. Synnaeve, J. Verbeek et al., "Resmlp: Feed-forward networks for image classification with data-efficient training," *IEEE Transactions on Pattern Analysis and Machine Intelligence*, 2022.
- [14] J. Kirkpatrick, R. Pascanu, N. Rabinowitz, J. Veness, G. Desjardins, A. A. Rusu, K. Milan, J. Quan, T. Ramalho, A. Grabska-Barwinska et al., "Overcoming catastrophic forgetting in neural networks," *Proceedings of the national academy of sciences*, vol. 114, no. 13, pp. 3521–3526, 2017.
- [15] M. Masana, X. Liu, B. Twardowski, M. Menta, A. D. Bagdanov, and J. van de Weijer, "Class-incremental learning: survey and performance evaluation on image classification," *IEEE Transactions on Pattern Analysis and Machine Intelligence*, vol. 45, no. 5, pp. 5513–5533, 2023.
- [16] A. Douillard, Y. Chen, A. Dapogny, and M. Cord, "Plop: Learning without forgetting for continual semantic segmentation," in *Proceedings of the IEEE/CVF Conference on Computer Vision and Pattern Recognition*, 2021, pp. 4040–4050.
- [17] C.-B. Zhang, J.-W. Xiao, X. Liu, Y.-C. Chen, and M.-M. Cheng, "Representation compensation networks for continual semantic segmentation," in *Proceedings of the IEEE/CVF Conference on Computer Vision and Pattern Recognition*, 2022, pp. 7053–7064.
- [18] K. He, X. Zhang, S. Ren, and J. Sun, "Deep residual learning for image recognition," in *Proceedings of the IEEE conference on computer vision and pattern recognition*, 2016, pp. 770–778.
- [19] S. Chen, E. Xie, G. Chongjian, R. Chen, D. Liang, and P. Luo, "Cyclempl: A mlp-like architecture for dense prediction," in *International Conference on Learning Representations*, 2022.
- [20] E. Xie, W. Wang, Z. Yu, A. Anandkumar, J. M. Alvarez, and P. Luo, "Segformer: Simple and efficient design for semantic segmentation with transformers," *Advances in Neural Information Processing Systems*, vol. 34, pp. 12 077–12 090, 2021.
- [21] B. Peng, W. Wang, J. Dong, and T. Tan, "Optimized 3d lighting environment estimation for image forgery detection," *IEEE Transactions on Information Forensics and Security*, vol. 12, no. 2, pp. 479–494, 2017.
- [22] Y. Liu, Q. Guan, X. Zhao, and Y. Cao, "Image forgery localization based on multi-scale convolutional neural networks," in *Proceedings of the 6th ACM workshop on information hiding and multimedia security*, 2018, pp. 85–90.
- [23] D. Cozzolino and L. Verdoliva, "Noiseprint: A cnn-based camera model fingerprint," *IEEE Transactions on Information Forensics and Security*, vol. 15, pp. 144–159, 2019.
- [24] J. Wang, Z. Wu, J. Chen, X. Han, A. Shrivastava, S.-N. Lim, and Y.-G. Jiang, "Objectformer for image manipulation detection and localization," in *Proceedings of the IEEE/CVF Conference on Computer Vision and Pattern Recognition*, 2022, pp. 2364–2373.
- [25] S.-J. Ryu, M. Kirchner, M.-J. Lee, and H.-K. Lee, "Rotation invariant localization of duplicated image regions based on zernike moments," *IEEE Transactions on Information Forensics and Security*, vol. 8, no. 8, pp. 1355–1370, 2013.

- [26] D. Cozzolino, G. Poggi, and L. Verdoliva, "Efficient dense-field copy-move forgery detection," *IEEE Transactions on Information Forensics and Security*, vol. 10, no. 11, pp. 2284–2297, 2015.
- [27] X. Bi and C.-M. Pun, "Fast reflective offset-guided searching method for copy-move forgery detection," *Information Sciences*, vol. 418, pp. 531–545, 2017.
- [28] —, "Fast copy-move forgery detection using local bidirectional coherency error refinement," *Pattern Recognition*, vol. 81, pp. 161–175, 2018.
- [29] J. Li, X. Li, B. Yang, and X. Sun, "Segmentation-based image copy-move forgery detection scheme," *IEEE Transactions on Information Forensics and Security*, vol. 10, no. 3, pp. 507–518, 2015.
- [30] C.-M. Pun, X.-C. Yuan, and X.-L. Bi, "Image forgery detection using adaptive oversegmentation and feature point matching," *IEEE transactions on information forensics and security*, vol. 10, no. 8, pp. 1705–1716, 2015.
- [31] E. Ardizzone, A. Bruno, and G. Mazzola, "Copy-move forgery detection by matching triangles of keypoints," *IEEE Transactions on Information Forensics and Security*, vol. 10, no. 10, pp. 2084–2094, 2015.
- [32] E. Silva, T. Carvalho, A. Ferreira, and A. Rocha, "Going deeper into copy-move forgery detection: Exploring image telltales via multi-scale analysis and voting processes," *Journal of Visual Communication and Image Representation*, vol. 29, pp. 16–32, 2015.
- [33] C. Wang, Z. Huang, S. Qi, Y. Yu, G. Shen, and Y. Zhang, "Shrinking the semantic gap: spatial pooling of local moment invariants for copy-move forgery detection," *IEEE Transactions on Information Forensics and Security*, vol. 18, pp. 1064–1079, 2023.
- [34] A. Vaswani, N. Shazeer, N. Parmar, J. Uszkoreit, L. Jones, A. N. Gomez, L. Kaiser, and I. Polosukhin, "Attention is all you need," *Advances in neural information processing systems*, vol. 30, 2017.
- [35] A. Dosovitskiy, L. Beyer, A. Kolesnikov, D. Weissenborn, X. Zhai, T. Unterthiner, M. Dehghani, M. Minderer, G. Heigold, S. Gelly *et al.*, "An image is worth 16x16 words: Transformers for image recognition at scale," in *International Conference on Learning Representations*.
- [36] S. Zheng, J. Lu, H. Zhao, X. Zhu, Z. Luo, Y. Wang, Y. Fu, J. Feng, T. Xiang, P. H. Torr *et al.*, "Rethinking semantic segmentation from a sequence-to-sequence perspective with transformers," in *Proceedings of the IEEE/CVF conference on computer vision and pattern recognition*, 2021, pp. 6881–6890.
- [37] N. Carion, F. Massa, G. Synnaeve, N. Usunier, A. Kirillov, and S. Zagoruyko, "End-to-end object detection with transformers," in *Computer Vision—ECCV 2020: 16th European Conference, Glasgow, UK, August 23–28, 2020, Proceedings, Part I 16*. Springer, 2020, pp. 213–229.
- [38] R. Strudel, R. Garcia, I. Laptev, and C. Schmid, "Segformer: Transformer for semantic segmentation," in *Proceedings of the IEEE/CVF international conference on computer vision*, 2021, pp. 7262–7272.
- [39] T. Meinhardt, A. Kirillov, L. Leal-Taixe, and C. Feichtenhofer, "Trackerformer: Multi-object tracking with transformers," in *Proceedings of the IEEE/CVF conference on computer vision and pattern recognition*, 2022, pp. 8844–8854.
- [40] H. Chen, Y. Wang, T. Guo, C. Xu, Y. Deng, Z. Liu, S. Ma, C. Xu, C. Xu, and W. Gao, "Pre-trained image processing transformer," in *Proceedings of the IEEE/CVF Conference on Computer Vision and Pattern Recognition*, 2021, pp. 12 299–12 310.
- [41] S. He, H. Luo, P. Wang, F. Wang, H. Li, and W. Jiang, "Transreid: Transformer-based object re-identification," in *Proceedings of the IEEE/CVF international conference on computer vision*, 2021, pp. 15 013–15 022.
- [42] T. Yu, X. Li, Y. Cai, M. Sun, and P. Li, "S2-mlp: Spatial-shift mlp architecture for vision," in *Proceedings of the IEEE/CVF Winter Conference on Applications of Computer Vision*, 2022, pp. 297–306.
- [43] Q. Hou, Z. Jiang, L. Yuan, M.-M. Cheng, S. Yan, and J. Feng, "Vision permutator: A permutable mlp-like architecture for visual recognition," *IEEE Transactions on Pattern Analysis and Machine Intelligence*, vol. 45, no. 1, pp. 1328–1334, 2022.
- [44] D. Lian, Z. Yu, X. Sun, and S. Gao, "As-mlp: An axial shifted mlp architecture for vision," in *International Conference on Learning Representations*.
- [45] M. De Lange, R. Aljundi, M. Masana, S. Parisot, X. Jia, A. Leonardis, G. Slabaugh, and T. Tuytelaars, "A continual learning survey: Defying forgetting in classification tasks," *IEEE transactions on pattern analysis and machine intelligence*, vol. 44, no. 7, pp. 3366–3385, 2021.
- [46] S.-A. Rebuffi, A. Kolesnikov, G. Sperl, and C. H. Lampert, "icarl: Incremental classifier and representation learning," in *Proceedings of the IEEE conference on Computer Vision and Pattern Recognition*, 2017, pp. 2001–2010.
- [47] H. Shin, J. K. Lee, J. Kim, and J. Kim, "Continual learning with deep generative replay," *Advances in neural information processing systems*, vol. 30, 2017.
- [48] A. Chaudhry, M. Ranzato, M. Rohrbach, and M. Elhoseiny, "Efficient lifelong learning with a-gem," in *International Conference on Learning Representations*, 2018.
- [49] Z. Li and D. Hoiem, "Learning without forgetting," *IEEE transactions on pattern analysis and machine intelligence*, vol. 40, no. 12, pp. 2935–2947, 2017.
- [50] A. Mallya and S. Lazebnik, "Packnet: Adding multiple tasks to a single network by iterative pruning," in *Proceedings of the IEEE conference on Computer Vision and Pattern Recognition*, 2018, pp. 7765–7773.
- [51] A. A. Rusu, N. C. Rabinowitz, G. Desjardins, H. Soyer, J. Kirkpatrick, K. Kavukcuoglu, R. Pascanu, and R. Hadsell, "Progressive neural networks," *arXiv preprint arXiv:1606.04671*, 2016.
- [52] T. Feng, M. Wang, and H. Yuan, "Overcoming catastrophic forgetting in incremental object detection via elastic response distillation," in *Proceedings of the IEEE/CVF Conference on Computer Vision and Pattern Recognition*, 2022, pp. 9427–9436.
- [53] B. Yang, X. Deng, H. Shi, C. Li, G. Zhang, H. Xu, S. Zhao, L. Lin, and X. Liang, "Continual object detection via prototypical task correlation guided gating mechanism," in *Proceedings of the IEEE/CVF Conference on Computer Vision and Pattern Recognition*, 2022, pp. 9255–9264.
- [54] L. Yin, J. M. Perez-Rua, and K. J. Liang, "Sylph: A hypernetwork framework for incremental few-shot object detection," in *Proceedings of the IEEE/CVF Conference on Computer Vision and Pattern Recognition*, 2022, pp. 9035–9045.
- [55] F. Cermelli, M. Mancini, S. R. Bulò, E. Ricci, and B. Caputo, "Modeling the background for incremental learning in semantic segmentation," in *Proceedings of the IEEE/CVF Conference on Computer Vision and Pattern Recognition*, 2020, pp. 9233–9242.
- [56] C. Shang, H. Li, F. Meng, Q. Wu, H. Qiu, and L. Wang, "Incrementer: Transformer for class-incremental semantic segmentation with knowledge distillation focusing on old class," in *Proceedings of the IEEE/CVF Conference on Computer Vision and Pattern Recognition*, 2023, pp. 7214–7224.
- [57] T. Kalb and J. Beyerer, "Principles of forgetting in domain-incremental semantic segmentation in adverse weather conditions," in *Proceedings of the IEEE/CVF Conference on Computer Vision and Pattern Recognition*, 2023, pp. 19 508–19 518.
- [58] K. Nguyen and S. Todorovic, "ifs-rcnn: An incremental few-shot instance segmenter," in *Proceedings of the IEEE/CVF Conference on Computer Vision and Pattern Recognition*, 2022, pp. 7010–7019.
- [59] T.-Y. Lin, P. Dollár, R. Girshick, K. He, B. Hariharan, and S. Belongie, "Feature pyramid networks for object detection," in *Proceedings of the IEEE conference on computer vision and pattern recognition*, 2017, pp. 2117–2125.
- [60] H. Zhao, J. Shi, X. Qi, X. Wang, and J. Jia, "Pyramid scene parsing network," in *Proceedings of the IEEE conference on computer vision and pattern recognition*, 2017, pp. 2881–2890.
- [61] Q. Hou, L. Zhang, M.-M. Cheng, and J. Feng, "Strip pooling: Rethinking spatial pooling for scene parsing," in *Proceedings of the IEEE/CVF conference on computer vision and pattern recognition*, 2020, pp. 4003–4012.
- [62] B. Wen, Y. Zhu, R. Subramanian, T.-T. Ng, X. Shen, and S. Winkler, "Coverage—a novel database for copy-move forgery detection," in *2016 IEEE international conference on image processing (ICIP)*. IEEE, 2016, pp. 161–165.
- [63] T.-Y. Lin, M. Maire, S. Belongie, J. Hays, P. Perona, D. Ramanan, P. Dollár, and C. L. Zitnick, "Microsoft coco: Common objects in context," in *Computer Vision—ECCV 2014: 13th European Conference, Zurich, Switzerland, September 6–12, 2014, Proceedings, Part V 13*. Springer, 2014, pp. 740–755.
- [64] J. Xiao, J. Hays, K. A. Ehinger, A. Oliva, and A. Torralba, "Sun database: Large-scale scene recognition from abbey to zoo," in *2010 IEEE computer society conference on computer vision and pattern recognition*. IEEE, 2010, pp. 3485–3492.